Journal of Materials Chemistry C

Accepted Manuscript

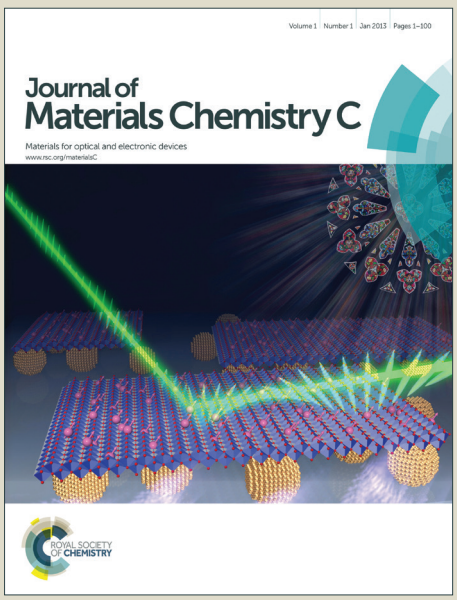

ROYAL SOCIETY OF CHEMISTRY

www.rsc.org/materialsC

Cite this: DOI: 10.1039/c0xx00000x

www.rsc.org/xxxxxx

ARTICLE TYPE

Deep ultraviolet to near-infrared photoresponse from glucose-derived graphene oxide

Sin Ki Lai,[a] Libin Tang,[ab] Yeung Yu Hui,[ab] Chi Man Luk[ab] and Shu Ping Lau*[ab]

Received (in XXX, XXX) XthXXXXXXXXX 20XX, Accepted Xth XXXXXXXXX 20XX

DOI: 10.1039/b000000x

Graphene oxide (GO) was synthesized by a hydrothermal method using glucose solution as sole reagent. The wavelength-dependent photoresponse of the GO was investigated by fabricating metal-GO-metal photodetectors. The devices demonstrated broadband photoresponse from 290 to 1610 nm covering deep ultraviolet (UV) to near-infrared (NIR), which is the broadest spectral range yet demonstrated on GO. The response times of the photodetectors in the UV and visible range are about 100 ms, which are at least one order of magnitude faster than photodetectors based solely on GO reported previously. The responsivity of the photodetector can be as high as 23.6 mA/W in the visible range. The wavelength-dependent photoresponse is closely related to the absorption characteristic of the GO. Potential for self-powered GO based photodetector is first demonstrated, the device shows prominent photoresponse at zero bias. The GO based photodetectors pave the way for developing low-cost, broadband, self-powered as well as spectrally tuneable photodetectors.

Introduction

Graphene has recently been popularly investigated for application in photodetection due to its broad absorption spectrum[1], which is a consequence of zero band gap and strong interband transition. High carrier mobility in graphene also enables high speed operation up to 500 GHz.[2] However, the one-atom thick graphene results in low absorbance, thus pure graphene photodetectors typically show low responsivity, in the order of mA/W.[2-3] Some recent works have therefore incorporated graphene with high optical absorption nanostructures, e.g. quantum dots, to form hybrid photodetectors.[4-6] Graphene plays the role of carrier transport layer in these devices by utilizing the superior electrical conductivity over quantum dots, but its wide band absorption characteristic cannot be expressed. Wide band photodetection has many potential applications in imaging, sensing and communication.[7] Graphene oxide (GO) and reduced graphene oxide (RGO), which are graphene derivatives decorated with oxygen functional groups on its basal plane and edges[8], also shows wide band asborption.[9] In addition, they can be produced in multilayer and in bulk quantity at a time.[10]

A few studies had employed GO and RGO in photodetection. Some used GO or RGO as the only active material.[11-15] Qi *et al*. demonstrated GO photoresponse in UV, visible light and NIR[13], but unstable photocurrent was found upon UV illumination, which is attributed to the reduction of GO in UV. Chitara *et al*. demonstrated GO photoresponse at 360 nm[11] and 1550 nm[12] but without visible light investigation. In addition, the variations of photoresponse over different excitation wavelengths have not been addressed clearly. Other works formed Schottky photodiode between RGO and silicon[9,16] or integrated GO with nanostructures[17-19], but the contribution of GO in photodetection was blurred by silicon and nanostructures in these studies. It is important to understand the wavelength-dependent photoresponse in GO, and the origin of such dependence, in order to ascertain the practical application of GO in photodetection.

In this work, a vertical junction photodetector employing GO as the only active material was fabricated. The wavelength-dependent photodetection of GO was investigated in detail. The GO was produced by hydrothermal processing of glucose solution followed by thermal annealing.[20] The conductivity and charge mobility of the GO can be tuned over wide range by using different annealing temperatures as tabulated in Table S1 (ESI†). Our GO photodetectors demonstrate stable photoresponse in UV and visible light with response time of about 100 ms and 130 ms, respectively. The response time in this range is at least one order of magnitude faster than the previously reported GO photodetectors.[11,13,15]

Experimental

Preparation of graphene oxide

GO was prepared by hydrothermal processing of glucose solution following a procedure described elsewhere.[20] Glucose powder was dissolved in deionized water to give 0.5 M glucose solution. About 40ml glucose solution was transferred to a 50 ml Teflon-lined autoclave with a diameter of 3.5 cm and was heated at 180 ^{o}C for 3 – 4 hours. The reaction mixture was cooled overnight to room temperature. Multilayer GO forms at the solution-air interface and can be transferred to arbitrary substrate by dip-coating. The as-grown GO film is continuous over the solution surface, limited only by the cross sectional area of the autoclave.

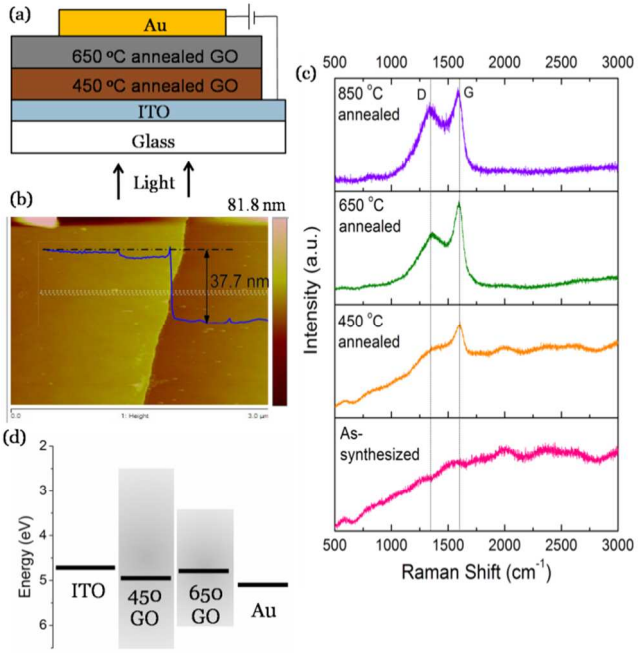

Fig. 1 (a) Schematic structure of the GO photodetector. The bias condition of the photodetector is indicated. (b) AFM height profile of a 650GO with a synthesis time of 4hrs. Film thickness is 37.7nm. (c) Raman spectra of the GO with different annealing temperatures. (d) Flat energy band diagram of the device.

Thickness of the as-grown GO can be controlled by varying the hydrothermal time, temperature and concentration of glucose solution. The hydrothermal temperature and concentration of glucose solution were kept constant at 180 °C and 0.5 M respectively. The as-grown GO is an insulator. Thermal annealing was used to transform the GO to a semiconductor.

Device fabrication

The schematic structure of the device is shown in Fig. 1(a). The GO under hydrothermal synthesis of 3 hours was dip-coated onto indium tin oxide (ITO) coated glass. The GO/ITO was annealed under vacuum in 450 °C for 8 minutes. Another GO film with a synthesis time of 4 hours was dip-coated onto copper foil, and was then annealed under vacuum in 650 °C for 8 minutes. High annealing temperature may increase the resistance of ITO, [21] thus 650 °C annealed GO is transferred after annealing. The above GOs are designated as 450GO and 650GO respectively, similarly for GO of other annealing temperatures in this work. The 650GO/Cu was floated in 1 M $FeCl_3$ solution to etch away copper. The etching time was 1 day. The resulted 650GO film was transferred to DI water for several times to wash away the etchant. The 650GO was then dip-coated onto the prepared 450GO/ITO structure. Au of about 100 nm thick was thermally evaporated through a shadow mask as the top electrode. ITO serves as the bottom electrode in the device.

Results and discussion

Characterization of GO films

Fig. S1(a) (ESI†) shows the atomic force microscopy (AFM) image of a 450GO. The film deposited on the substrate by dip-coating is uniform, and has a root-mean-square (RMS) roughness of 1.1 nm. The film thickness is 36 nm according to Fig. S1(c). Fig. S1(b) shows the AFM image of a 650GO transferred from Cu foil to a Si substrate. The roughness of the GO increases after transference with a RMS roughness of 51nm. The film thickness is 37.7 nm as shown in Fig. 1(b). According to the device structure (Fig. 1(a)), the total thickness of the GO is about 70 nm.

Raman spectra of the GO with various annealing temperatures are shown in Fig. 1(c). The GO generally shows two characteristic peaks: the G peak at about 1600 cm^{-1}, which corresponds to the in-plane vibrations of sp^2 carbon, and the D peak at about 1350 cm^{-1}, is related to the disorder in graphene plane, due to scattering at the edges of defects.[22-23] The as-synthesized GO has a strong fluorescence background with no characteristic peak. At 450 °C annealing, the G peak appears, showing the formation of sp^2 domains, and the GO still exhibits strong fluorescence background. Phase change is clearly observed as the annealing temperature increases to 650 °C and 850 °C. The fluorescence background disappears. Prominent G and D peaks are observed.

Fig. 2(a) shows the UV-Vis absorption spectra for different annealing temperatures of the GO. The GO exhibits two major features. First is a shoulder at around 300 nm, which corresponds to the n to π^* transition of C=O bond, and is attributed to the sp^3 bonding in GO.[24-25] Second feature is a peak at around 200 nm, which corresponds to the π to π^* transition of sp^2 C-C bond.[24-25] Two changes of the peak are observed as annealing proceeds. Firstly, the peak broadens. Second, the peak shows a clear red shift from 198 to 266 nm, from the as-synthesized GO to the 1000GO. The peak shift is found to be linear with annealing temperature as shown in the inset of Fig. 2(a). This redshift had also been reported before and is attributed to the increase in sp^2 content in the GO as annealing proceeds.[24-25] As seen from Fig. S2 (ESI†), the enhanced absorption at visible and NIR as the degree of reduction increases[26] reveals that the absorbance, and hence the photoresponse, of the GO is spectrally tunable by controlling the degree of reduction. It would be pointed out in later section that the responsivity of the GO photodetector is largely determined by the absorbance at the corresponding wavelength.

To evaluate the chemical function groups present in the GO, Fourier Transform Infrared Spectroscopy (FTIR) was performed. The FTIR spectra of 450GO, 650GO and their analysis are provided in Fig. S3 (ESI†). The spectra reveal the presence of C=C, C-H, C=O, C-O and -OH bonds that are typically found in GO.[20, 27]

Fig. 2(b) shows the Tauc plot of the GO for different annealing temperatures. The intercept of the dotted line is a reference to the optical band gap of the GO, although GO does not have a clear cut band gap due to its mixed sp^2 and sp^3 nature.[28-30] In addition to the large number of trap states resulted from the oxygen functional groups and defects induced by annealing.[31-32] From Fig. 2(b), for the as-synthesized GO, 450GO, 650GO and 850GO, the optical band gap is estimated to be 4.45, 4.07, 2.71 and 2.41 eV respectively. Optical band gap of GO decreases with the degree of reduction, which agrees with previous works.[33-34] These values indicate that the optical band gap of the GO is tuneable over wide range.

The flat energy band diagram of the device is shown in Fig. 1(d).

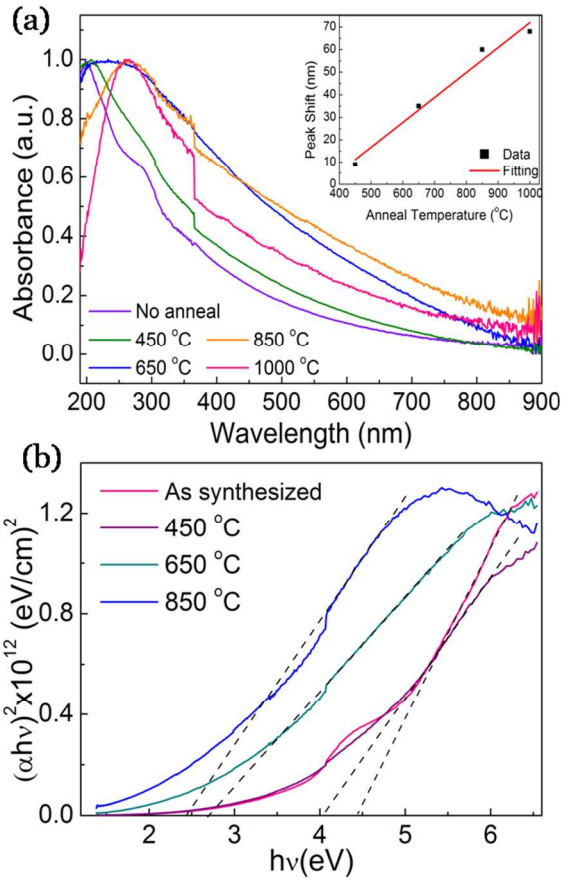

Fig. 2 (a) Normalized UV-Vis spectra of the as-synthesized GO and 450GO, 650GO, 850GO and 1000GO. The abrupt jump at 365 nm is due to the change of light source in the spectrometer but not the samples. Inset shows the linear relation between shift in π to π^* peak and annealing temperature. (b) Tauc plot for the as-synthesized GO and 450GO, 650GO and 850GO. The optical band gap is estimated to be 4.45, 4.07, 2.71 and 2.41 eV respectively.

Work function of GO increases as the oxygen content increases.[35-36] Work functions of GO and RGO have been reported to be 4.9-4.96eV and 4.79-4.88eV respectively.[37-38] HOMO for GO and RGO obtained from ultraviolet photoelectron spectroscopy (UPS) are ~1.5 eV and ~1.1 eV below the work function respectively.[39] Using the band gap values obtained from Fig. 2(b), the LUMO of the GOs are determined. It can be seen from Fig. 1(c) that 450GO acts as an effective electron blocking layer[37] to suppress photogenerated electrons diffuse from LUMO of 650GO towards the ITO electrode. The 650GO serves as an effective absorption layer in the device, as seen from its stronger absorption in Fig. S2.

As a comparison, another set of photodetectors with 700GO replacing 650GO were fabricated. Photoresponse of the 700GO device is provided in Fig. S4 (ESI†). Although GO of higher annealing temperature shows higher absorbance, the increased electrical conductivity of the 700GO results in higher dark current at 1V bias, which reduces the specific detectivity (D^*) and on/off ratio as tabulated in Table 1. D^* and on/off ratio are given by [16, 40, 41] $D^*=RA^{1/2}(2qI_{dark})^{-1/2}$ and on/off = I_{light}/I_{dark} where R is the responsivity at a particular wavelength, q is the electron charge, A is the effective area of the device, I_{light}, I_{dark} are current under light and dark respectively. The low detectivity and on/off ratio would degrade the ability of photodetectors to detect low light power. Therefore, 650GO is applied in this device.

Table 1

D* and on/off ratio of 700GO/450GO and 650GO/450GO device structures under 410 nm excitation at 3.1 mW

Device structure	D*(10^7cmHz$^{1/2}$W^{-1})	on/off
700GO/450GO	2.33	1.01
650GO/450GO	3.31	1.46

Device performance

In all the electrical measurements, the electrodes are connected according to Fig. 1(a). The current-voltage (I-V) characteristic of the device is shown in Fig. 3(a). A nonlinear I-V is observed, which indicates the formation of Schottky barrier in the device.[42] Schottky barrier creates internal electric field. Upon absorption of photons, electron-hole pairs are generated. Internal electric field helps separate the electron-hole pairs and hinders their recombination. Charge carriers are swept by electric field in opposite direction towards the electrodes and results in photocurrent.

The temporal responses of the device under UV, visible light and NIR excitations are shown in Fig. 3(b)-(d) respectively. The photoresponse covers from 290 to 1610 nm, which is the broadest spectral range yet demonstrated on photodetectors that applied GO as the only active material, the photoresponse thus can be solely attributed to the GO. Photoresponse of the GO at 290 nm was measured with a planar structure device as shown in Fig. S5 (ESI†), as ITO is opaque to 290 nm radiation. Electrical measurements were obtained in ambient condition using a Keithley 2400 meter. The bias voltage was 1V unless otherwise specified. The light sources include 290, 375, 410, 660, 940 nm light emitting diodes (LEDs) and 1610 nm laser diode. The detail specification of the light sources can be found in ESI†. The device shows good photoresponse under UV and visible light. Photocurrent saturates quickly after light is on, and drops quickly back to dark current level when light is off. In UV and visible light, the absence of an exponentially saturating rise and fall edge in the provided time scale indicates a small contribution from the slow diffusion component of the charge carriers, while fast drift component of charge carriers dominates in photodetection.[43]

The relationship between light intensity and photocurrent was investigated. Power of the light source was measured with an optical power meter. The effective illumination area was fixed at 7 mm^2 in all measurements by passing light through a shadow mask. In Fig. 3(e), the photocurrent is plotted against light intensiy in log-scale under 410 nm excitation. Data are fitted with the power law $I_{ph} = \alpha P^{\theta}$, where I_{ph} is the photocurrent, P is the light intensity and α is a constant. The value of θ obtained from fitting is 0.991. The monotonic variation of photocurrent between 10^{-6} – 10^{-1} Wcm^{-2} shows that the photodetectors can effectively distinguish light intensity in this range.

To demonstrate the reproducibility of the photoresponse, a square voltage of frequency 0.43 Hz was supplied to a 410 nm LED. The

Cite this: DOI: 10.1039/c0xx00000x

www.rsc.org/xxxxxx

ARTICLE TYPE

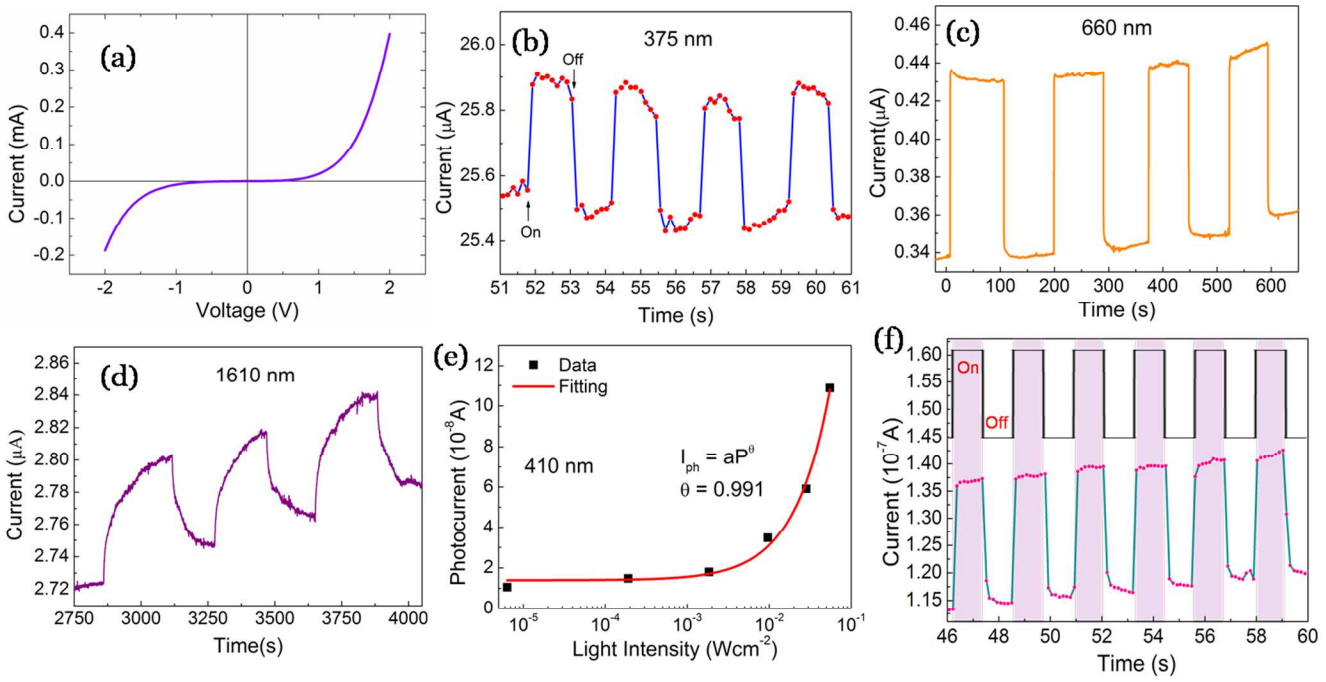

Fig. 3 (a) *I-V* characteristic of the device in the dark. Temporal photoresponse under (b) UV, (c) visible light and (d) NIR excitation. (e) Photocurrent against log-scale of the light intensity under 410 nm excitation. Red line indicates fitting with the power law. (f) Photoresponse under periodic on-off cycles of 0.43 Hz at 410 nm, demonstrating the reproducibility of the photodetectors.

corresponding photoresponse is shown in Fig. 3(f). The output current follows closely the signal from the light source, demonstrating a fast response. The photoresponse is stable with no appreciable change in the magnitude of photocurrent over all on/off cycles in the measurement. The dark current is increasing with time under an applied voltage, which is also observed in Fig. 3(c), and 3(d). The origin for the continuous increase in dark current with time is not very clear. However, a changing in dark current with time is commonly observed in photodetectors.[44, 45] As the magnitude of the photocurrent is almost constant for many on/off cycles as shown in Table S2 (ESI†), the increasing in dark current with time should not be related to the reduction in GO due to light illumination.[13]

Next, important figures of merit of photodetectors, including responsivity and response time, were characterized. The device demonstrated very different photoresponse in NIR as compared to UV and visible light. Responsivity (R) measures the amount of photocurrent (I_{ph}) generated by a unit of optical power (P). It is given by the equation $R=I_{ph}/P$. Responsivity in log-scale as a function of excitation wavelength is given in Fig. 4(a). The powers at different wavelengths were maintained at 1 – 5 mW. It is found that the responsivity generally decreases with wavelength from 375 to 940 nm, and is fitted with an exponential function. The inset of Fig. 4(a) shows the responsivity in linear scale against wavelength. It can be seen from the inset the responsivity exhibits a similar trend with the UV-Vis absorption spectrum in Fig. 2(a).

This shows that the absorption of the GO at a particular wavelength is a critical factor to the corresponding responsivity. The wide band photodetection of the device is attributed to the broad range absorption of the GO. The GO exhibits a weak but non-zero absorption in NIR which results in the low responsivity in NIR.

Fig. 4(b) shows the responsivity of the device as a function of light intensity. As shown in the figure, the highest responsivity of the device under 1V bias at 410 nm is 23.6 mA/W, which is higher than the RGO/Si nanowires hybrid photodetectors[9] and is comparable to other GO based photodetectors.[11, 13] As opposed to photocurrent in Fig. 3(e), the responsivity decreases with increasing light intensity, This is also observed in some quantum dot photodetectors.[5, 6]

The relationship between bias voltage with photocurrent and responsivity are also investigated. Fig. 4(c) and 4(d) show respectively the photocurrent and responsivity as a function of bias voltage under different light intensities at 410 nm. For a wide range of light intensities, both photocurrent and responsivity increases with bias voltage. This indicates that bias voltage can effectively suppress the recombination of electron-hole pairs, and increase the efficiency of extracting charge carriers to the electrodes.

Cite this: DOI: 10.1039/c0xx00000x

www.rsc.org/xxxxxx

ARTICLE TYPE

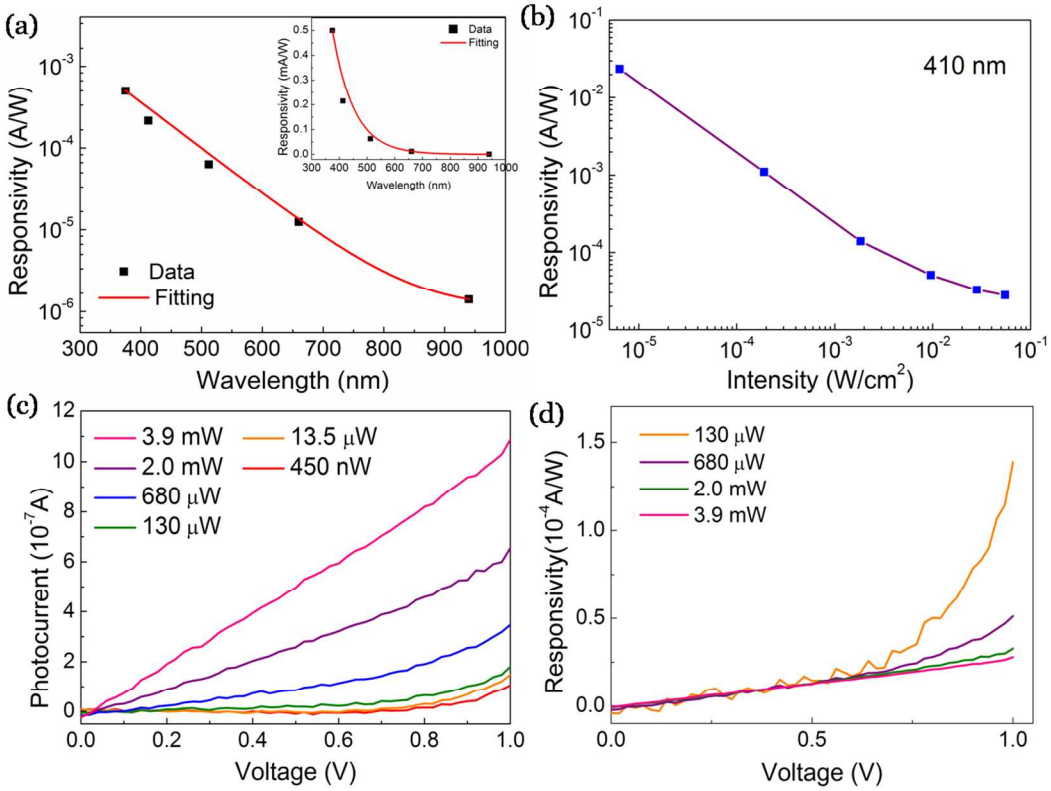

Fig. 4 (a) Log-scale of the responsivity as a function of wavelength. Inset shows the linear scale of the responsivity against wavelength. The inset exhibits similar trend with the absorption spectrum of GO. (b) Log-log scale of responsivity as a function of light intensity. (c) Photocurrent as a function of bias voltage under a series of optical powers. (d) Responsivity as a function of bias voltage under a series of optical powers.

Response time is another important parameter for photodetectors. Rise (fall) time is defined as time interval from 10% (90%) to 90% (10%) of saturated photocurrent with respect to the dark current after light is on (off).The rise and fall times under UV, visible light and NIR are tabulated in Table 2. Fig. 5(a) shows the rise time, fall time analysis and time constant fittings of a 660 nm excitation.

It is noted that the response time in UV (~105ms) and visible light (130ms) range is at least one order of magnitude faster than the previously reported photodetectors that applied GO as the only active material, in which the time constants are reported to be ~30min[11] and 5 – 20s[13] in UV and visible light respectively. In addition, the photocurrent does not reach complete saturation in these works. The faster response in this work compared to the previous work is partly attributed to the small separation between the electrodes in the device in which the active layer is only 70 nm thick. Thus it reduces the distance travelled by the carriers upon reaching the electrodes, when compared with ref. 11 where the electrode separation is 2 mm.

Response time is longer under NIR excitation than visible light and UV, which is also reported in previous work.[13] It is clearly observed in Fig. 3(d) where under NIR excitation, an obvious fast drift component as represented by the sharp rise is followed by a slower component represented by the exponential saturation of photocurrent. A possible reason for the slow response time at NIR is trapping of charge carriers. Some works reported that C=O functional groups and defects in GO may trap charge carriers[46], which result in a negative photocurrent[11], and slow response time.[13] Due to the weak absorption in NIR, for a constant number of trapping sites in GO, a larger proportion of photogenerated carriers from NIR excitation are trapped. Trapping increases the recombination lifetime of charge carriers[47],

Table 2

Rise and fall times under different excitation wavelengths

Wavelength (nm)	Rise time	Fall time
375	~105ms	~105ms
660	130ms	152ms
1610	78.13s	70.99s

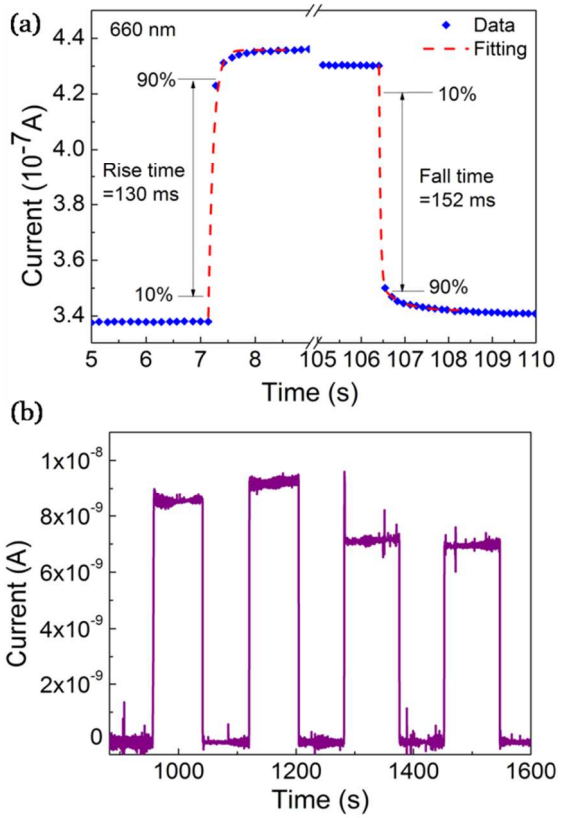

Fig. 5 (a) Rise time and fall time analysis of photoresponse under 660 nm excitation. Red dashed curves are the exponential fittings for determination of rise and decay time constants. (b) Photoresponse under zero bias voltage at 410 nm.

longer travelling time to electrodes is enabled, which manifests as a significantly longer response time.

Lastly, the possibility for self-powered GO based photodetectors is investigated for the first time. As shown in Fig. 5(b), the device demonstrates prominent and fast photoresponse under zero bias voltage. Compared to 1V bias, under same condition of 410 nm excitation at 3.1 mW, the magnitude of photocurrent decreases but the on/off ratio increases from 1.46 at 1V bias to ~10^3 at zero bias. Although bias can increase the responsivity of the device, self-powered photodetectors are more desirable when considering application under harsh condition and weight reduction.[48] This shows that the GO based device has potential application as self-powered photodetectors.

Conclusions

Vertical junction photodetector employing GO as the only active material shows fast response time of ~105 ms in UV and 130 ms in visible light. The responsivity reaches 23.6 mA/W at 410 nm and 1 V bias. The device shows significantly lower responsivity and longer response time in NIR region. These wavelength dependent properties are related to the unique absorption characteristic of the GO, which is a finite but much lower absorbance at NIR region. The low absorbance in NIR can be enhanced by increasing the annealing temperature of GO, which implies that the GO photodetectors may be spectrally tuneable. Under zero bias, the device shows fast response with an on/off ratio ~1000. The GO shows promising application for high performance UV and visible light self-powered photodetectors.

Acknowledgements

This work was financially supported by the Research Grants Council of Hong Kong (Project No. PolyU 5006/12P), PolyU grants (Project Nos. G-YN10, 1-ZV8N, and 1-ZE14) and National Natural Science Foundation of China (Grant no. 11374250)

Notes and references

[a]*Department of Applied Physics, The Hong Kong Polytechnic University, Hung Hom, Kowloon, HKSAR.*
[b]*The Hong Kong Polytechnic University Shenzhen Research Institute, Shenzhen 518057, China.*
E-mail: apsplau@polyu.edu.hk

†Electronic Supplementary Information (ESI) available: [Hall measurements of resistivity and carrier mobility for different annealing temperatures of the GO, AFM images, FTIR spectra, deep UV photoresponse, details of light sources]. See DOI: 10.1039/b000000x/

1 R. R. Nair, P. Blake, A. N. Grigorenko, K. S. Novoselov, T. J. Booth, T. Stauber, N. M. R. Peres and A. K. Geim, *Science*, 2008, **320**, 1308.
2 F. Xia, T. Mueller, Y. M. Lin, A. Valdes-Garcia and P. Avouris, *Nat. Nanotechnol.*, 2009, **4**, 839 – 843.
3 T. Mueller, F. Xia and P. Avouris, *Nat. Photonics*, 2010, **4**, 297-301.
4 G. Konstantatos, M. Badioli, L. Gaudreau, J. Osmond, M. Bernechea, F. P. G. de Arquer, F. Gatti and F. H. L. Koppens, *Nat. Nanotechnol.*, 2012, **7**, 363-368.
5 S. H. Cheng, T. M. Weng, M. L. Lu, W. C. Tan, J. Y. Chen and Y. F. Chen,*Scientific Reports*, 2013, **3**, 2694.
6 Z. Sun, Z. Liu, J. Li, G.Tai, S. P. Lau and F. Yan, *Adv. Mater.*, 2012, **24**, 5878-5883.
7 C. H. Liu, Y. C. Chang, T. B. Norris and Z. Zhong, *Nat. Nanotechnol.*, 2014, **9**, 273-278.
8 D. R. Dreyer, S. Park, C. W. Bielawski and R. S. Ruoff, *Chem. Soc. Rev.*, 2010, **39**, 228-240.
9 Y. Cao, J. Zhu, J. Xu, J. He, J. L. Sun, Y. Wang and Z. Zhao, *Small*, 2014, DOI: 10.1002/smll.201303339.
10 D. Li, M. B. Müller, S. Gilje, R. B. Kaner and G. G. Wallace, *Nat. Nanotechnol.*, 2008, **3**, 101-105.
11 B. Chitara, S. B. Krupanidhi, and C. N. R. Rao, *Appl. Phys. Lett.*, 2011, **99**, 113114.
12 B. Chitara, L. S. Panchakarla, S. B. Krupanidhi and C. N. R. Rao, *Adv. Mater.*, 2011, **23**, 5419-5424.
13 X. Qi, X. Zou, Z. Huang, L. Ren, G. Hao, Y. Liu, X. Wei and J. Zhong, *Appl. Surf. Sci.*, 2013, **266**, 332-336.
14 S. Ghosh, B. K. Sarker, A. Chunder, L. Zhai and S. I. Khondaker, *Appl. Phys. Lett.*, 2010, **96**, 163109.
15 S. K. Chang-Jian, J. R. Ho, J. W. J. Cheng and Y. P. Hsieh, *AIP Advances*, 2012, **2**, 022104.
16 M. Zhu, X. Li, Y. Guo, X. Li, P. Sun, X. Zang, K. Wang, M. Zhong, D. Wu and H. Zhu, *Nanoscale*, 2014, **6**, 4909-4914.
17 A. Radoi, A. Iordanescu, A. Cismaru, M. Dragoman and D. Dragoman, *Nanotechnology*, 2010, **21**, 455202.
18 Y. Lin, K. Zhang, W. Chen, Y. Liu, Z. Geng, J. Zeng, N. Pan, L. Yan, X. Wang and J. G. Hou, *ACS Nano*, 2010, **4**, 3033-3038.
19 H. Chang, Z. Sun, K. Y. F. Ho, X. Tao, F. Yan, W. M. Kwok and Z. Zheng, *Nanoscale*, 2011, **3**, 258-264.
20 L. Tang, X. Li, R. Ji, K. S. Teng, G. Tai, J. Ye, C. Wei and S. P. Lau, *J. Mater. Chem.*, 2012, **22**, 5676-5683.
21 N. Nishimoto, Y. Yamada, Y. Ohnishi, N. Imawaka and K. Yoshino, *Phys. Status Solidi A*, 2013, **210**, 589-593.

22 L. G. Cançado, A. Jorio, E. M. Ferreira, F. Stavale, C. A. Achete, R. B. Capaz, M. V. O. Moutinho, A. Lombardo, T. S. Kulmala and A. C. Ferrari, Nano Lett., *Nano Letters*, 2011,**11**, 3190-3196.

23 A. C. Ferrari and J. Robertson, *Phys. Rev. B*, 2000, **61**, 14095.

24 Y. Zhang, H. L. Ma, Q. Zhang, J. Peng, J. Li, M. Zhai and Z. Z. Yu, *J. Mater. Chem.*, 2012, **22**, 13064-13069.

25 Q. Shou, J. Cheng, L. Zhang, B. J. Nelson and X. Zhang, *J. Solid State Chem.*, 2012, **185**, 191-197.

26 P. V. Kumar, N. M. Bardhan, S. Tongay, J. Wu, A. M. Belcher and J. C. Grossman, *Nat. Chem.*, 2014, **6**, 151-158.

27 C. Liu, F. Hao, X. Zhao, Q. Zhao, S. Luo and H. Lin, *Sci. Rep*., 2014, **4**, 3965.

28 G. Eda, Y.Y. Lin, C. Mattevi, H. Yamaguchi, H. A. Chen, I. S. Chen, C. W. Chen and M. Chhowalla, *Adv. Mater.*, 2010, **22**, 505-509.

29 D. Joung, S. I. Khondaker, J. Phys. Chem. C, 2013, 117, 26776−26782.

30 C. Gómez-Navarro, R. T. Weitz, A. M. Bittner, M. Scolari, A. Mews, M. Burghard and K. Kern, *Nano Lett.*, 2007,**7**, 3499-3503.

31 C. Mattevi, G. Eda, S. Agnoli, S. Miller, K. A. Mkhoyan, O. Celik, D. Mastrogiovanni, G. Granozzi, E. Garfunkel, and M. Chhowalla, *Adv. Funct. Mater.*, 2009, **19**, 2577-2583.

32 S. Kaniyankandy, S. N. Achary, S. Rawalekar and H. N. Ghosh, *J. Phys. Chem. C*, 2011, **115**, 19110-19116.

33 H. Chang, Z. Sun, Q. Yuan, F. Ding, X. Tao, F. Yan and Z. Zheng, *Adv. Mater.*, 2010, **22**, 4872-4876.

34 Y. Shen, S. Yang, P. Zhou, Q. Sun, P. Wang, L. Wan, J. Li, L. Chen, X. Wang, S. Ding and D. W. Zhang, *Carbon*, 2013, **62**, 157-164.

35 Z. Yin, S. Wu, X. Zhou, X. Huang, Q. Zhang, F. Boey and H. Zhang, *Small*, 2010, **6**, 307-312.

36 M. Mishra, R. K. Joshi, S. Ojha, D. Kanjilal, and T. Mohanty, *J. Phys. Chem. C*, 2013, **117**, 19746-19750.

37 S. S. Li, K. H. Tu, C. C. Lin, C. W. Chen and M. Chhowalla, *ACS Nano*, 2010, **4**, 3169-3174.

38 J. M. Yun, J. S. Yeo, J. Kim, H. G. Jeong, D. Y. Kim, Y. J. Noh, S. S. Kim, B. C. Ku and S. I. Na, *Adv. Mater.*, 2011, **23**, 4923-4928.

39 G. Singh, D. S. Sutar, V. D. Botcha, P. K. Narayanam, S. S. Talwar, R. S. Srinivasa and S. S. Major, *Nanotechnology*, 2013, **24**, 355704.

40 C. DeCusatis, I. P. Kaminow, in *The Optical Communications Reference*, 1st ed., Academic Press, 2010, p.184.

41 M. Tyagi, M. Tomar and V. Gupta, *J. Mater. Chem. C*, 2014,**2**, 2387-2393.

42 X. Wu, M. Sprinkle, X. Li, F. Ming, C. Berger and W. A. de Heer,*Phys. Rev. Lett.*, 2008, **101**, 026801.

43 J. P. Clifford, G. Konstantatos, K. W. Johnston, S. Hoogland, L. Levina and E. H. Sargent, *Nat. Nanotechnol.*, 2009, **4**, 40-44.

44 N. Liu, H. Tian, G. Schwartz, J. B. H. Tok, T. L. Ren and Z. Bao, *Nano Letters*, 2014, DOI:10.1021/nl500443j.

45 K. Zheng, F. Meng, L. Jiang, Q. Yan, H. H. Hng and X. Chen, *Small*, 2013, **9**, 2076-2080.

46 H. Chang, Z. Sun, M. Saito, Q. Yuan, H. Zhang, J. Li, Z. Wang , T. Fujita, F. Ding, Z. Zheng, F. Yan, H. Wu, M. Chen and Y. Ikuhara, *ACS Nano*, 2013, **7**, 6310-6320.

47 G. Konstantatos, I. Howar, A. Fischer, S. Hoogland, J. Clifford, E. Klem, L. Levina and E. H. Sargent, *Nature*, 2006, **442**, 180-183.

48 Z. Zhan, L. Zheng, Y. Pan, G. Sun and L. Li, *J. Mater. Chem.*, 2012, **22**, 2589.

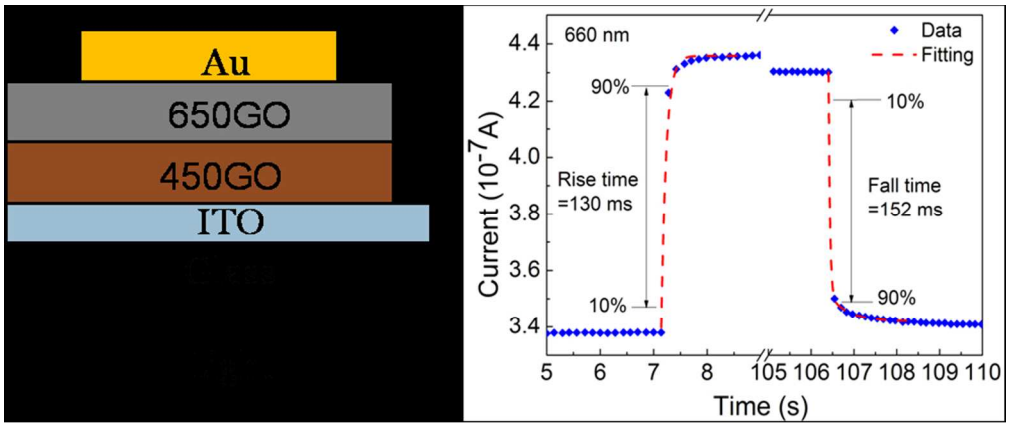

Deep ultraviolet to near infrared photodetector based on glucose-derived graphene oxide nanosheets.
167x70mm (150 x 150 DPI)